How curvature-generating proteins build scaffolds on membrane nanotubes

Mijo Simunovic[a,b,c,d,e,1,2], Emma Evergren[f,3], Ivan Golushko[g], Coline Prévost[a,4], Henri-François Renard[h,5], Ludger Johannes[h], Harvey T. McMahon[f], Vladimir Lorman[g], Gregory A. Voth[b,c,d,e], and Patricia Bassereau[a,i,1]

[a]Laboratoire Physico Chimie Curie, Institut Curie, PSL Research University, CNRS UMR168, F-75005 Paris, France; [b]Department of Chemistry, The University of Chicago, Chicago, IL 60637; [c]Institute for Biophysical Dynamics, The University of Chicago, Chicago, IL 60637; [d]James Franck Institute, The University of Chicago, Chicago, IL 60637; [e]Computation Institute, The University of Chicago, Chicago, IL 60637; [f]Laboratory of Molecular Biology, Medical Research Council, Cambridge CB2 0QH, United Kingdom; [g]Laboratoire Charles Coulomb, UMR 5221 CNRS, Université de Montpellier, F-34095 Montpellier, France; [h]Chemical Biology of Membranes and Therapeutic Delivery Unit, Institut Curie, PSL Research University, CNRS UMR3666, INSERM U1143, F-75005 Paris, France; and [i]Sorbonne Universités, Université Pierre et Marie Curie, Université Paris 6, F-75005, Paris, France

Edited by James H. Hurley, University of California, Berkeley, CA, and accepted by Editorial Board Member K. C. Garcia August 9, 2016 (received for review May 2, 2016)

Bin/Amphiphysin/Rvs (BAR) domain proteins control the curvature of lipid membranes in endocytosis, trafficking, cell motility, the formation of complex subcellular structures, and many other cellular phenomena. They form 3D assemblies that act as molecular scaffolds to reshape the membrane and alter its mechanical properties. It is unknown, however, how a protein scaffold forms and how BAR domains interact in these assemblies at protein densities relevant for a cell. In this work, we use various experimental, theoretical, and simulation approaches to explore how BAR proteins organize to form a scaffold on a membrane nanotube. By combining quantitative microscopy with analytical modeling, we demonstrate that a highly curving BAR protein endophilin nucleates its scaffolds at the ends of a membrane tube, contrary to a weaker curving protein centaurin, which binds evenly along the tube's length. Our work implies that the nature of local protein–membrane interactions can affect the specific localization of proteins on membrane-remodeling sites. Furthermore, we show that amphipathic helices are dispensable in forming protein scaffolds. Finally, we explore a possible molecular structure of a BAR-domain scaffold using coarse-grained molecular dynamics simulations. Together with fluorescence microscopy, the simulations show that proteins need only to cover 30–40% of a tube's surface to form a rigid assembly. Our work provides mechanical and structural insights into the way BAR proteins may sculpt the membrane as a high-order cooperative assembly in important biological processes.

protein scaffold | BAR proteins | membrane curvature | self-assembly | endocytosis

Curvature of lipid membranes plays important roles in the cell. It allows dynamic cellular phenomena, such as trafficking or cell division, and it can also mediate the interactions among many membrane-bound proteins (1, 2). Proteins containing a Bin/Amphiphysin/Rvs (BAR) domain participate in numerous membrane-curving processes, such as endocytosis, trafficking, motility, the formation of T-tubules, cytokinesis, and so on (3, 4). BAR domains are characterized by a crescent shape whose curvature, length, and binding affinity to the membrane are distinct among different members (4–6). Many BAR proteins also contain amphipathic helices that shallowly insert into the bilayer.

BAR proteins generate curvature as a combination of (*i*) adhesive electrostatic interactions via their BAR domain and (*ii*) the insertion of amphipathic helices. Additionally, BAR proteins can associate into highly ordered assemblies on the membrane, thus collectively altering its shape and mechanics (7–10). Precisely how they assemble and affect the membrane is argued to depend on the surface density of proteins, membrane tension, and membrane shape (11). On a flat membrane at a low surface density, BAR proteins can form strings and a meshlike network, which can give rise to budding and tubulation (12–16). At a sufficiently high protein density, they affect the mechanical properties of the membrane and stabilize membrane nanotubes (7, 10, 17–20).

An assembly of BAR proteins on cylindrical membranes has so far only been visualized using EM (e.g., refs. 8, 9, and 21). Although these studies provide important and detailed assessments of how BAR domains may interact with one another on curved membranes as a packed protein arrangement, membrane tubules in those experiments were generated typically from highly charged liposomes exposed to very high protein concentrations. In the cell, especially in the context of endocytosis, protein concentration is not high enough to induce appreciable spontaneous tubulation, nor would such a mechanism be beneficial to the cell. Importantly, a tightly packed assembly of BAR proteins would preclude the recruitment of many other proteins required in endocytosis and trafficking.

Significance

Lipid membranes are dynamic assemblies, changing shape on nano- to micron-sized scales. Some proteins can sculpt membranes by organizing into a molecular scaffold, dictating the membrane's shape and properties. We combine microscopy, mathematical modeling, and simulations to explore how Bin/Amphiphysin/Rvs proteins assemble to form scaffolds on nanotubes. We show that the way protein locally deforms the membrane affects where it will nucleate before making a scaffold. In this process, the protein's amphipathic helices—which shallowly insert into the membrane—seem dispensable. Surprisingly, the scaffold forms at low protein density on the nanotube. We simulate a structure of protein scaffolds at molecular resolution, shedding light on how these proteins may sculpt the membrane to facilitate important dynamic events in cells.

Author contributions: M.S., G.A.V., and P.B. designed research; M.S., I.G., and V.L. performed research; E.E., I.G., H.-F.R., L.J., H.T.M., and V.L. contributed new reagents/analytic tools; M.S., E.E., C.P., H.T.M., G.A.V., and P.B. analyzed data; and M.S., E.E., G.A.V., and P.B. wrote the paper.

The authors declare no conflict of interest.

This article is a PNAS Direct Submission. J.H.H. is a Guest Editor invited by the Editorial Board.

[1]To whom correspondence may be addressed. Email: msimunovic@rockefeller.edu or patricia.bassereau@curie.fr.

[2]Present address: Center for Studies in Physics and Biology, The Rockefeller University, New York, NY 10065.

[3]Present address: Centre for Cancer Research and Cell Biology, Queen's University Belfast, Belfast BT7 1NN, United Kingdom.

[4]Present address: Department of Genetics and Complex Diseases, T. H. Chan School of Public Health, and Department of Cell Biology, Harvard Medical School, Boston, MA 02115.

[5]Present address: Institut des Sciences de la Vie, Université Catholique de Louvain, B-1348 Louvain-la-Neuve, Belgium.

This article contains supporting information online at www.pnas.org/lookup/suppl/doi:10.1073/pnas.1606943113/-/DCSupplemental.

To achieve close packing, protein–protein interactions were implicated to be important, namely the lateral interactions between neighboring BAR domains in F-BAR proteins (8) or between N-terminal amphipathic helices in N-BAR proteins (9). It is unclear whether BAR proteins in endocytosis and trafficking cooperatively shape the membrane by virtue of specific protein–protein interactions or whether they assemble as a result of a more general membrane-mediated mechanism. Moreover, it is important to understand how BAR proteins assemble at much lower protein surface densities and on membrane compositions that much more likely resemble those found within the cell.

We hypothesize that BAR proteins can oligomerize on a membrane nanotube at densities much lower than close packing owing to membrane-mediated attractions. We refer to this structure as a protein scaffold. It is to be noted that the term "scaffold" is often used to describe a single BAR domain, imprecisely termed the scaffolding domain. Here, a scaffold represents a 3D rigid assembly of multiple proteins that adheres to the membrane and affects the shape and properties of the membrane.

In this work, we combine in vitro reconstitution, fluorescent microscopy, mechanical measurements, and analytical modeling to describe the mechanism by which BAR proteins assemble on membrane nanotubes to form a scaffold. We also demonstrate that rigid protein scaffolds form at much lower surface densities than full packing. We simulate the protein scaffold at molecular resolution using coarse-grained (CG) molecular dynamics (MD).

Finally, because the relative contribution of BAR domain versus amphipathic helices in inducing curvature is still highly debated, we explore how these domains contribute to the scaffold formation. To this end, we tested three proteins with well-distinguished structural features: endophilin A2 (an N-BAR protein containing four amphipathic helices), endophilin A2 mutants, β2-centaurin (a classical BAR domain with no amphipathic helices), and epsin 1 (a protein that binds membranes via an amphipathic helix in its epsin N-terminal homology domain).

Results

Endophilin Scaffold Initiates at the Base of a Tube. To study the interactions of BAR proteins with a cylindrical membrane, we used a previously developed micromanipulation setup (7). In the experiment, we pull a nanotube from a giant unilamellar vesicle (GUV) using optical tweezers. A nanotube connected to the base membrane is a typical configuration characteristic of some endocytic processes, such as in a clathrin-independent endocytic mechanism mediated by endophilin (22, 23). The vesicle is held by a micropipette whose aspiration pressure sets the membrane tension, implicitly tube radius, in the absence of proteins (24, 25) (*SI Methods*). Thus, we have a direct control of the initial radius of curvature, which in our case ranges from ∼10 nm to ∼100 nm (7). With another micropipette we inject the protein near the tube, starting from low vesicle tension. The N-BAR domain of the WT endophilin A2 and β2 centaurin (BAR + pleckstrin homology domain) were fluorescently labeled so that we could directly observe their binding to the membrane with confocal microscopy. By measuring the lipid and the protein fluorescence, we can calculate the tube radius and the protein's surface density, respectively (7) (Fig. S1 and *SI Methods*). Therefore, at the same time, we observe how proteins affect the shape of the membrane, while controlling membrane tension and membrane curvature.

We prepared GUVs using a total lipid brain extract, supplemented with 5% (mol/mol) PI(4,5)P_2. Because such a natural composition has not yet been used for quantitative mechanical measurements (26, 27), we confirmed that the membrane curvature scales with GUV tension as theoretically expected for fluid membranes (25) and that these vesicles are not undergoing phase separation (28) (*SI Text* and Figs. S2 and S3).

First, we studied how the N-BAR of endophilin A2 (29, 30) (Fig. S4) forms a scaffold on a membrane tube, by injecting the protein at 0.5–2.5 μM (dimeric concentration in the pipette). Note that due to diffusion the concentration of the protein near the GUV is approximately half that in the pipette (31). Endophilin showed a remarkable specificity for the base of a pulled nanotube, binding first either at the interface with the vesicle or with the trapped bead (Fig. 1*A*). Note that the two interfaces are morphologically equivalent, having the same saddle-like membrane geometry. Out of 59 experiments, endophilin first bound to the GUV–tube interface in 53 of them, while also simultaneously binding to the interface with the bead in 27 experiments. In four cases, endophilin seemed to bind homogeneously along the tube where, possibly, the initial binding was not recorded sufficiently fast. Only in the two remaining cases considered as negative the protein first bound to a region other than the interface.

Shortly after binding, the region covered by endophilin continuously grew along the tube, eventually partially or fully covering it (Fig. 1 *A* and *B;* see *SI Text* for additional statistics). In most cases, the growth of the endophilin scaffold was linear and it ranged from ∼20 nm·s^{-1} to ∼300 nm·s^{-1} (Fig. 1*B*; see also Fig. S5 and Movie S1).

The marked reduction of the lipid fluorescence intensity underneath the protein (Fig. 1*A*, lipid channel) indicates that endophilin changes the tube radius independently of GUV tension. Hence, it forms a stable 3D structure that dictates the membrane curvature. Tube constriction has previously been observed with other members of the BAR family (7, 22, 32), although the dynamics of scaffold formation has not been captured. Binding and constriction under the scaffold are concomitant with the progressive drop in force required to hold the nanotube (Fig. 1*B*). A fully covered tube at low GUV tension imposes no force on the optical trap and undergoes buckling (see the deformation of the tube in the bottom panel of Fig. 1*A*; also see Movie S1). Of note, in the experiments the proteins are also bound to the GUV (see, e.g., Fig. 1*A*).

We observed no difference in the tube-binding behavior between the full-length endophilin A2 (N-BAR + SH3 domain) and only its N-BAR domain, indicating that the location of scaffold initiation is not determined by the protein's SH3 domain (Fig. S5).

Interestingly, sometimes at higher injected concentrations (>1.5 μM in the injection pipette) endophilin initially formed a

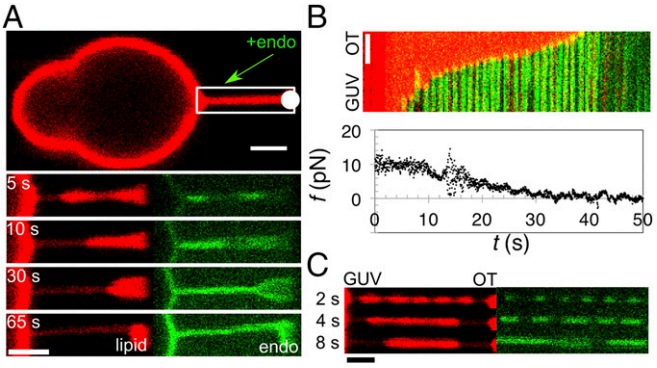

Fig. 1. Scaffolding by endophilin A2. (*A*) Endophilin A2 N-BAR domain (endo) (amino acids 1–247) binds to the tube's base and forms a scaffold that continuously grows along the tube [note the progressive constriction in the tube radius from the GUV toward the optical trap (OT, white circle)]. (*B*) A kymogram of scaffold growth from the GUV to the bead (fluorescence dims near the end as the tube buckles in and out of focus). Lipid and protein channels are overlaid. The plot shows tube-retraction force, *f*, as a function of time, *t*. The *x* axis of the kymogram coincides with the *x* axis of the plot. (*C*) Time lapse of a striated pattern induced by endophilin A2 N-BAR domain. $t = 0$ marks the time when protein was detected on the tube. (All scale bars, 2 μm.)

striated pattern on the nanotube, marked by a brief (few seconds) beading instability (Fig. 1*C*, observed in 6 out of 31 experiments). The striation rapidly coarsened, leading to a growth of the scaffold from both bases of the tube. To some extent, this behavior is reminiscent of the way dynamin binds to membrane tubes. Dynamin binds in a striated pattern and affects the membrane force. In the case of dynamin, however, the membrane force changes only after the entire tube is covered with the protein (33, 34), contrary to endophilin, in which case a decrease in the force is seen immediately upon binding.

Role of Protein Subdomains in Scaffolding. We then aimed to examine how changing the intrinsic curvature and the presence of amphipathic helices affect the scaffolding dynamics. β2 centaurin provides a good testing ground, because it is one of few BAR proteins without an N-terminal amphipathic helix (35). Additionally, the BAR domain of centaurin is much shallower than that of endophilin, as judged by their atomic models (*SI Text* and Fig. S4). Contrary to endophilin, centaurin bound homogeneously along the nanotube, with no detectable preference to the neck (Fig. 2*A*). Nevertheless, there was a reduction in the membrane force during binding, leading to a buckling instability at low tension (Fig. 2*A*). Importantly, binding of the protein changed the curvature of the tube, even though the aspiration pressure remained the same. Fig. 2*B* shows an example where binding of β2 centaurin dilates a 30-nm tube by ∼20 nm. Furthermore, once the scaffold forms, either by centaurin or endophilin, the tube radius remains constant; its magnitude is characteristic of the protein, but independent of GUV tension (Fig. 2*C*). Namely, the tube scaffolded by centaurin is approximately four times wider than the one scaffolded by endophilin (42.5 nm compared with 10 nm, Table 1). This observation is in line with the difference in intrinsic curvatures of their BAR domains (Fig. S4).

The formation of a scaffold by either endophilin or centaurin also drastically changes the mechanics of the membrane, evident from the systematic reduction in the equilibrium tube force for all tested membrane tensions (Fig. 2*C*). Based on previous analytical modeling, the force of a scaffolded tube—characterized by a constant radius—is expected to linearly depend on GUV tension, whereas a bare membrane is expected to have a square-root dependence (7, 25). Indeed, the membrane force of protein-covered tubes in experiments shown in Fig. 2*C* displays a linear dependence on tension (Fig. S6), thus confirming the formation of a scaffold by a measurement independent of tube radius.

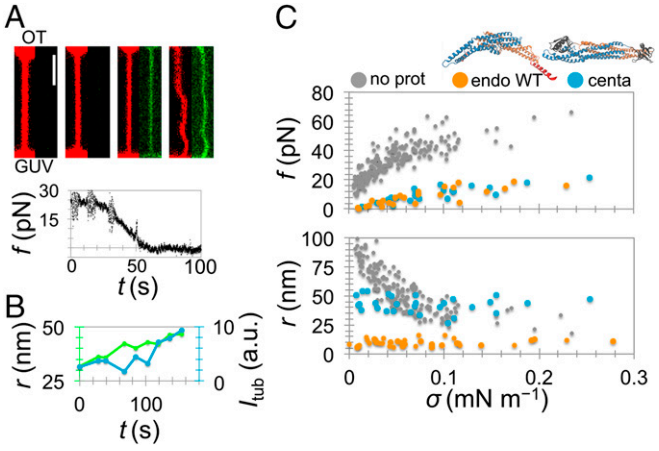

Fig. 2. Scaffolding by N-BAR versus BAR domains. (*A*) β2 centaurin BAR domain (amino acids 1–384) binds evenly along the tube (red, lipid and green, protein) and causes a decrease in tube-retraction force, *f*, just like endophilin. (Scale bar, 2 μm.) (*B*) Dilation of a narrow tube induced by a scaffold of β2 centaurin BAR domain (overlaid are fluorescence intensity of the protein on the tube, I_{tub}, and the tube radius, *r*, deduced from lipid fluorescence). (*C*) The mechanics of the reference membrane ($n = 45$) and after the formation of a scaffold by endophilin A2 WT (endo WT, $n = 7$) and β2 centaurin (centa, $n = 5$). Tube force, *f*, measured from the optical trap; tube radius, *r*, measured from lipid fluorescence.

Table 1. Radius of scaffolded tubes measured from lipid fluorescence

Radius, *r*	endo WT	endo ΔH0	endo mut	centa
nm (*N*)	9.8 ± 2.8 (10)	21.4 ± 11.6 (7)	19.9 ± 3.0 (7)	42.5 ± 7.0 (5)

Values are means ± SD with *N* measurements in parentheses. centa, β2 centaurin; endo ΔH0, endophilin A2 with truncated N-terminal helices; endo mut, endophilin A2 N-BAR domain E37K, D41K; endo WT, WT endophilin A2 (data from the full-length protein and the N-BAR domain are pooled).

To further investigate the role of amphipathic helices versus the BAR domain in scaffolding, we constructed two endophilin mutants. In the first, we truncated the N-terminal amphipathic helix of the full-length endophilin A2 (endo ΔH0). In the second, we mutated one glutamate and one aspartate from the membrane-binding region of endophilin A2 N-BAR domain into lysines (E37K and D41K) (endo mut), which enhances the binding strength of the BAR domain to the membrane. Both variants constricted the tube starting from an interface (Fig. 3, red fluorescence) and decreased the force (Fig. 3, white plot) and tube radius (Table 1) in the same manner as the WT. This observation confirms that the N-terminal amphipathic helices are not necessary for the formation of the scaffold or, interestingly, for the preferential binding to the tube's base in these experiments, although the scaffolding rate seems slower (Fig. 3).

Finally, we tested the full-length epsin 1, another important endocytic protein that participates in the initial stages of clathrin-mediated endocytosis (36). Epsin does not contain a BAR domain; instead, it binds and bends the membrane via an amphipathic helix. There was a clear mechanical effect upon the injection of epsin 1, characterized by a systematic reduction in both the equilibrium tube force and the tube radius for a wide range of membrane tensions, indicating that the protein induces positive spontaneous curvature (7) (Fig. S7). Similarly to centaurin, the constriction did not start from the base; rather, it appeared homogenous along the tube length. Unlike endophilin and centaurin, the force never decreased to zero and so we never

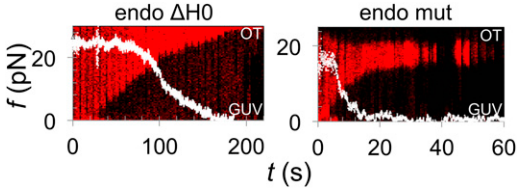

Fig. 3. Amphipathic helices do not determine the scaffold initiation site. Shown are force plots (white) overlaid on kymograms of lipid fluorescence of a membrane nanotube (red marker) during binding and scaffolding by endophilin mutants. As before, the formation of a scaffold is evident from tube constriction. (*Left*) Scaffolding by endophilin A2 with truncated N-terminal helices (endo ΔH0). (*Right*) Scaffolding by endophilin A2 N-BAR domain E37K, D41K (endo mut).

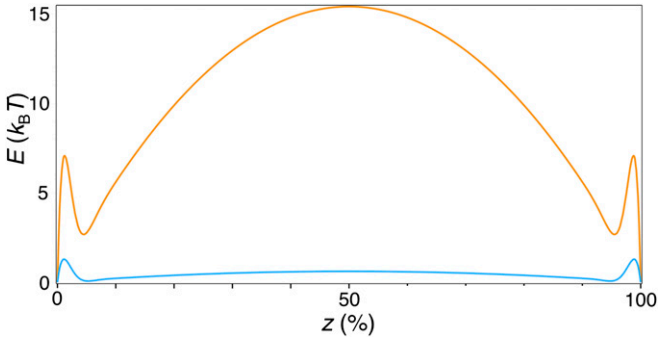

Fig. 4. Strongly curving proteins nucleate at the base of a pinned and fluctuating tube. Mathematical model: strain energy variation profile, *E*, as a function of the axial position on the tube, *z* (in percentage of total length), plotted using $\Delta\sigma = 0.25\%$ (orange) and 0.05% (blue), $\kappa = 50\ k_BT$, $L/r = 100$.

observed buckling. The square-root scaling of the force with membrane tension (Fig. S6) indicates that no scaffold forms, even at very high protein concentration (10-fold higher than minimal endo WT concentration that makes a scaffold). In summary, amphipathic helices alone may remodel the membrane, as in the case of epsin. However, the anisotropic BAR domain is critical for forming a rigid scaffold.

Pinning a Fluctuating Tube Determines the Protein's Binding Site. So far, we demonstrated that BAR proteins lacking amphipathic helices may form scaffolds just as N-BAR proteins; however, it is still unclear what determines the nucleation site of the protein. Our experiments cannot provide a general mechanism to answer this question and so we developed a mathematical model of BAR proteins interacting with a membrane tube. Several models have already been proposed for an equivalent system (7, 37), but those models did not capture the location of protein nucleation. We extend these models in two ways. First, we generalize the protein–membrane interactions by assuming that the proteins induce a local perturbation, expressed in terms of a tension or a pressure variation. Second, instead of taking periodic boundary conditions, we model a membrane tube pinned at its ends assuming that the radial displacement of the bilayer is strongly limited at the one end by the optical trap and at the other by the vesicle.

As we show in *SI Text* in detail, we decompose the free energy into the costs of (*i*) bending and (*ii*) stretching the membrane, supplemented by (*iii*) a term accounting for membrane–protein interactions and (*iv*) the energy associated with a point force keeping the membrane tubular (Eq. **S14**) (25, 37, 38). Solving the equation in the limit of low protein concentration, we obtain the mechanical strain energy variation (Eq. **S17**) induced by membrane–protein interactions, whose minima essentially indicate the binding sites of the protein. Importantly, the shape of this function strongly depends on the protein-induced local tension (or curvature) perturbation. When taking a local tension variation of $\Delta\sigma = 0.25\%$, the energy profile has a minimum at each of the tube's ends separated by a very high energy barrier at the tube's center (Fig. 4). Reducing the local perturbation fivefold to 0.05% lowers the barrier to $<1\ k_BT$ and thermal fluctuations dominate (Fig. 4; see also *SI Text* and Fig. S8).

According to our model, proteins that significantly affect the local structure of the membrane preferentially bind to the necks of a pinned fluctuating tube. This conclusion is in excellent agreement with our observations. Endophilin A2, displaying a much higher intrinsic curvature of its N-BAR domain (Fig. S4*A*) and having four amphipathic helices (Fig. 2 and Table 1), is expected to very strongly locally perturb the bilayer, which is why it clearly nucleates at the tube–vesicle interface. β2 centaurin, however, displays a shallow curvature of the BAR domain (Fig. 2 and Table 1) and lacks amphipathic helices (Fig. S4*B*), which is why it binds homogenously along the tube. Both endophilin mutants were found to localize at the tube's base. For the mutant that binds more strongly to the membrane this observation is not surprising in light of our theory. Surprisingly, however, endo ΔH0 is also found at the base despite lacking N-terminal helices. It seems that the shape and charge of endophilin's BAR domain and the short insert helices present at the BAR-domain dimerization interface impose sufficient local bilayer perturbation to determine the protein's localization.

Recall that our model is valid in the dilute limit, and therefore it cannot account for the emergence of the striated pattern that require a higher protein density. A previously developed model explaining FtsZ rings on tubes can be applied here instead (39). That model predicts that a higher protein concentration induces a uniformly unstable tube at a given tension, leading to a dynamic instability that promotes local protein condensates, separated by an energy barrier. Based on our experiments, this configuration is transient, because the scaffold readily covers the tube within a few seconds.

BAR Scaffold Is Not Densely Packed on the Tube. In previous sections we discussed the mechanism of protein nucleation and the mechanical aspects of protein scaffolds. We now explore the potential molecular structure of scaffolds after they have formed. Previous EM images and CG simulations have revealed that at very high protein to lipid ratios N-BAR proteins amphiphysin and endophilin very densely assemble on liposomes, transforming 100- to 400-nm vesicles into tubules and tubular networks (9, 19, 40). Prior fluorescence microscopy experiments have shown that N-BARs form scaffolds when their density on the GUV exceeds ~1,000 μm^{-2} (~5% areal fraction if taking 50 nm^2 as the area of the protein) (7, 10). We found a similar quantitative behavior for the BAR protein β2 centaurin. Namely, in our experiments, we measured an areal density of the protein dimer to be 3,600 ± 830 μm^{-2} on the GUV (18% coverage, $n = 5$; see *SI Text* for details on density measurements). As expected due to curvature sorting, the surface density on the tube was somewhat higher, measuring 7,400 ± 1,800 μm^{-2} (35% coverage). The surface density of dimeric endophilin A2 N-BAR domain on the tube was comparable, measuring 8,800 ± 5,300 μm^{-2} (43% coverage, $n = 4$), with a corresponding density on the GUV of 1,650 ± 750 μm^{-2} (8% coverage). Both protein measurements

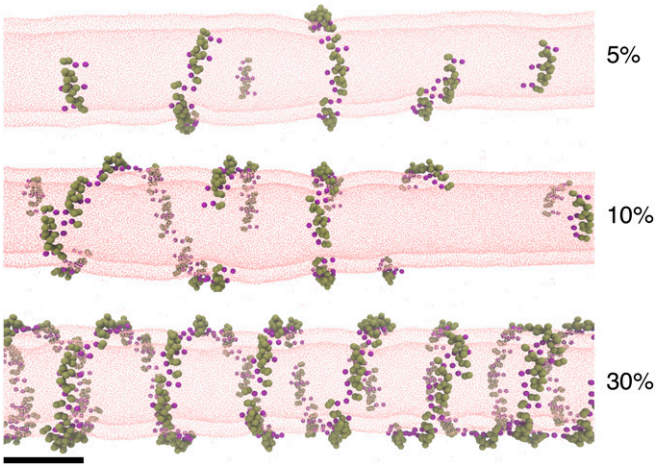

Fig. 5. Simulation of N-BAR domains on nanotubes. Shown are final snapshots of CG MD simulations of membrane tubes coated with N-BAR proteins at the indicated protein surface densities. (Scale bar, 20 nm.)

are comparable to 25% on the tube previously measured for amphiphysin (7).

Our experiments therefore indicate that proteins do not need to be densely packed to form a scaffold as seen in EM experiments in vitro. To understand the structure of the scaffold at molecular resolution, we performed CG MD simulations of endophilin's N-BAR domain on a 20-nm-wide lipid bilayer tube. We placed N-BARs at 5, 10, 30, and 40% surface coverage, starting either from a random or a tightly packed configuration, and carried out ∼30 million simulation time steps.

Regardless of the initial assembly of proteins and the protein density, we observed that N-BAR domains readily interacted with one another along their longitudinal axis, forming strings (Fig. 5). This arrangement resembles the membrane-mediated linear aggregation previously predicted for N-BAR proteins and, to a weaker degree, spherical particles (12–14, 41). Under confinement (on a flat or spherical surface), the proteins pack into a mesh (12); however, it seems that a tubular surface directs the proteins into a helix, with seven to eight N-BAR domains making a full helical turn (Fig. 5).

We note that in CG MD simulations the helix contiguously wraps the tubule at 30–40% protein coverage, in excellent agreement with the experimentally measured scaffold density. Once attaining this density, the proteins cease to exchange neighbors and the helix becomes quasistatic (Fig. 5; also see *SI Text* and Fig. S9).

Discussion

Two related curvature-generating proteins can initiate a scaffold at different membrane locations, as shown by our in vitro reconstituted system. Namely, an N-BAR protein endophilin nucleates at the tube's ends, whereas a BAR protein centaurin binds evenly along it. Our mathematical modeling predicts that specific binding to the saddle-shaped neck of a pinned and fluctuating membrane tube is a consequence of strong local membrane perturbations. An important conclusion from these observations is that the nature of local protein–membrane interactions can affect the specific initial localization of proteins on curved membranes and, thus, the dynamics of their assembly on membrane-remodeling sites.

Although the complexity of multiprotein interactions may divert the nucleation preference of BAR proteins in a cell, our findings seem to agree very well with previous in vivo studies of endocytosis. Immunoelectron microscopy of endophilin on clathrin-coated pits in cells at endogenous protein concentrations showed that endophilin indeed sits at the base of the clathrin coat (42). In the same study, in cells treated with a non-hydrolysable GTP, which form long dynamin-covered tubes, endophilin was again only found at the base of the coat (42). By contrast, dynamin was found all along the tubule's length.

Endophilin interacts with other proteins in a dynamic way. Namely, the tubulation efficiency and the amount of dynamin recruited to GUVs or lipid tubules are significantly increased by endophilin, and vice versa (42, 43). Furthermore, acutely perturbing endophilin using antibodies against the SH3 or the BAR domain stalled the formation of clathrin-coated pits before the sculpting of a narrow neck and the saddle (44, 45). Hence, endophilin could potentially play important roles in directing other endocytic proteins to their binding site.

Concerning protein's subdomains, the BAR domain seems crucial for the formation of a rigid scaffold. As previously demonstrated on a flat membrane, local membrane deformations mediate the interactions among BAR proteins and induce their assembly. The anisotropic shape of the BAR domain likely further facilitates an ordered packing and the formation of a scaffold. Therefore, a BAR domain is indeed a scaffolding domain, although not because a single protein imprints its shape on the membrane, but owing to a collective effect imposed by an ordered membrane-mediated helical assembly. Moreover, amphipathic helices seem dispensable in scaffolding; however, their role is still important in facilitating protein recruitment to the membrane (22) and in increasing the membrane's spontaneous curvature (Table 1). They may also have a role at the molecular level to help properly orient the BAR domains into a rigid scaffold, evidenced by the wide distribution of tubular radii when they are truncated (Table 1) (22), agreeing with previous work (9).

Importantly, our results show that a scaffold can form at much lower surface densities than full packing. Dense protein packing would be problematic for endocytosis. According to previous simulations, the shape of a basic unit of a BAR-domain lattice on the membrane affects the radius of the scaffold (18). Therefore, the radius of the tubule scaffolded by the same protein would be variable, depending on the way it formed the lattice, which seems unfavorable for endocytosis and trafficking, which require a tight curvature control. Indeed, tubule radii from different in vitro studies were infrequently different for the same protein. For example, tubule radii formed and scaffolded by amphiphysin 1 in vitro (measured between the membrane midplanes) were found to be 21 nm (35) and ∼11 nm (46), both based on EM imaging, compared with 7 nm measured by fluorescence microscopy (7). Based on our combined experimental and simulation data, under protein concentrations much lower than those used in EM imaging in vitro, BAR proteins do not build lattices on preformed tubes. Instead, they only cover 30–45% of the surface (depending on the protein), forming a stable and a rigid scaffold with constant curvature, bearing resemblance to in vivo EM images in which membrane tubules were created in the cell by endogenous protein concentrations (42, 47). In turn, this assembly provides structural integrity for endocytosis and leaves sufficient membrane area for the binding of accessory proteins crucial in the process (42, 46, 48).

Based on our work, we can propose different biologically relevant purposes for the N-BAR domain scaffolds. First, in endocytosis, they constrict the membrane tube between the endocytic vesicle and the underlying membrane, thus reducing the energy barrier for scission by dynamin (33) or by elongation forces (22). Second, highly curving proteins such as endophilin are specifically recruited to the neck, and so in clathrin-dependent endocytosis, where endophilin recruits dynamin to the tube (43), the scission site will be highly localized to the base of the coat. Third, scaffolds provide a powerful control of membrane curvature that may be used in forming complex cellular architectures, such as in the formation of T-tubules or the maintenance of mitochondrial shape, which require N-BAR proteins amphiphysin 2 (49) and endophilin B1 (50), respectively. The subtle differences in structures of these proteins give rise to a complexity in intracellular architectures and the highly dynamic behavior of the membrane. These differences are also likely the key way of modulating the function and localization of BAR proteins. We also expect that in the near future the higher-order organization of BAR proteins will be shown to be crucial in additional important membrane-remodeling phenomena.

Methods

Pulling Nanotubes and Making Protein Scaffolds. GUVs [95% total lipid brain extract (26), 5% (mol/mol) PI(4,5)P_2, supplemented with 0.1% di-stearoyl phosphatidyl ethanolamine-PEG(2000)-biotin and 1% BODIPY TR ceramide] were prepared by electroformation on Pt wires overnight at 4 °C in a salt-containing buffer (51). To pull a tube, the GUV was aspirated in a micropipette, brought in contact with a streptavidin-coated optically trapped bead, then gently pulled away. Proteins were injected near the tube with another micropipette. The aspiration pressure sets the membrane tension and the tube radius, r, in the absence of proteins, as $r = \sqrt{\kappa/2\sigma}$, where κ is membrane stiffness and σ is membrane tension (7, 24, 52–54). The tube force, f, was measured by videomicroscopy as $f = k_{OT}(a - a_0)$, where k_{OT} is the trap stiffness and a and a_0 are the current and the equilibrium bead positions, respectively. The r (in the presence or absence of proteins) was measured from

lipid fluorescence as $r = K_{tub} I_{tub} / I_{ves}$, where I_{tub} and I_{ves} are the fluorescence intensities of lipids in the tube and in the GUV, respectively, and $K_{tub} = 200 \pm 50$ nm is a previously measured calibration constant (7, 32).

CG MD Simulations. We used a solvent-free three-site CG lipid model (55) and a 26-site elastic network model of an N-BAR domain dimer of endophilin A1 (9) with protein-membrane interactions modeled using a Lennard-Jones potential as described previously (12). We simulated N-BARs on a lipid bilayer tube (150 nm in length and 20 nm in diameter interacting with its periodic images in the tube direction) at 5, 10, 30, and 40% surface coverage. The simulations were carried at a constant number of molecules, box volume, and temperature for ~30 million time steps at a time step of 12 fs using LAMMPS (56).

ACKNOWLEDGMENTS. We thank A. Callan-Jones for insightful discussions. This work was supported by National Institutes of Health Grant R01-GM063796 (to M.S. and G.A.V.), National Science Foundation Extreme Science and Engineering Discovery Environment Computational Resources (XSEDE) Grant TG-MCA94P017 (supercomputer Stampede), Agence Nationale pour la Recherche Grants ANR-11BSV201403 (to P.B.) and ANR-09BLAN283 (to H.-F.R. and L.J.), European Research Council Advanced Grant 340485 (to L.J.), and Medical Research Council Grant U105178795 (to E.E. and H.T.M.). M.S. was funded in part by a Chateaubriand Fellowship, a France and Chicago Collaborating in the Sciences grant, and the University Paris Diderot. The P.B. group belongs to the CNRS consortium CellTiss, the P.B. and L.J. groups belong to the LabEx CelTisPhyBio (ANR-11-LABX0038) and Paris Sciences et Lettres (ANR-10-IDEX-0001-02), and the V.L. group belongs to the LabEx NUMEV.

1. McMahon HT, Gallop JL (2005) Membrane curvature and mechanisms of dynamic cell membrane remodelling. *Nature* 438(7068):590–596.
2. Phillips R, Ursell T, Wiggins P, Sens P (2009) Emerging roles for lipids in shaping membrane-protein function. *Nature* 459(7245):379–385.
3. Mim C, Unger VM (2012) Membrane curvature and its generation by BAR proteins. *Trends Biochem Sci* 37(12):526–533.
4. Qualmann B, Koch D, Kessels MM (2011) Let's go bananas: Revisiting the endocytic BAR code. *EMBO J* 30(17):3501–3515.
5. Suetsugu S, Toyooka K, Senju Y (2010) Subcellular membrane curvature mediated by the BAR domain superfamily proteins. *Semin Cell Dev Biol* 21(4):340–349.
6. Rao Y, Haucke V (2011) Membrane shaping by the Bin/amphiphysin/Rvs (BAR) domain protein superfamily. *Cell Mol Life Sci* 68(24):3983–3993.
7. Sorre B, et al. (2012) Nature of curvature coupling of amphiphysin with membranes depends on its bound density. *Proc Natl Acad Sci USA* 109(1):173–178.
8. Frost A, et al. (2008) Structural basis of membrane invagination by F-BAR domains. *Cell* 132(5):807–817.
9. Mim C, et al. (2012) Structural basis of membrane bending by the N-BAR protein endophilin. *Cell* 149(1):137–145.
10. Shi Z, Baumgart T (2015) Membrane tension and peripheral protein density mediate membrane shape transitions. *Nat Commun* 6:5974.
11. Simunovic M, Voth GA, Callan-Jones A, Bassereau P (2015) When physics takes over: BAR proteins and membrane curvature. *Trends Cell Biol* 25(12):780–792.
12. Simunovic M, Srivastava A, Voth GA (2013) Linear aggregation of proteins on the membrane as a prelude to membrane remodeling. *Proc Natl Acad Sci USA* 110(51): 20396–20401.
13. Simunovic M, Voth GA (2015) Membrane tension controls the assembly of curvature-generating proteins. *Nat Commun* 6:7219.
14. Noguchi H (2016) Membrane tubule formation by banana-shaped proteins with or without transient network structure. *Sci Rep* 6:20935.
15. Traub LM (2015) F-BAR/EFC domain proteins: Some assembly required. *Dev Cell* 35(6): 664–666.
16. McDonald NA, Vander Kooi CW, Ohi MD, Gould KL (2015) Oligomerization but not membrane bending underlies the function of certain F-BAR proteins in cell motility and cytokinesis. *Dev Cell* 35(6):725–736.
17. Zhu C, Das SL, Baumgart T (2012) Nonlinear sorting, curvature generation, and crowding of endophilin N-BAR on tubular membranes. *Biophys J* 102(8):1837–1845.
18. Yu H, Schulten K (2013) Membrane sculpting by F-BAR domains studied by molecular dynamics simulations. *PLOS Comput Biol* 9(1):e1002892.
19. Cui H, et al. (2013) Understanding the role of amphipathic helices in N-BAR domain driven membrane remodeling. *Biophys J* 104(2):404–411.
20. Ramesh P, et al. (2013) FBAR syndapin 1 recognizes and stabilizes highly curved tubular membranes in a concentration dependent manner. *Sci Rep* 3:1565.
21. Pang X, et al. (2014) A PH domain in ACAP1 possesses key features of the BAR domain in promoting membrane curvature. *Dev Cell* 31(1):73–86.
22. Renard HF, et al. (2015) Endophilin-A2 functions in membrane scission in clathrin-independent endocytosis. *Nature* 517(7535):493–496.
23. Boucrot E, et al. (2015) Endophilin marks and controls a clathrin-independent endocytic pathway. *Nature* 517(7535):460–465.
24. Kwok R, Evans E (1981) Thermoelasticity of large lecithin bilayer vesicles. *Biophys J* 35(3):637–652.
25. Derényi I, Jülicher F, Prost J (2002) Formation and interaction of membrane tubes. *Phys Rev Lett* 88(23):238101.
26. Yu S, et al. (2006) Identification of phospholipid molecular species in porcine brain extracts using high mass accuracy of 4.7 Tesla Fourier transform ion cyclotron resonance mass spectrometry. *B Kor Chem Soc* 27(5):793–796.
27. Rawicz W, Olbrich KC, McIntosh T, Needham D, Evans E (2000) Effect of chain length and unsaturation on elasticity of lipid bilayers. *Biophys J* 79(1):328–339.
28. Sorre B, et al. (2009) Curvature-driven lipid sorting needs proximity to a demixing point and is aided by proteins. *Proc Natl Acad Sci USA* 106(14):5622–5626.
29. Gallop JL, et al. (2006) Mechanism of endophilin N-BAR domain-mediated membrane curvature. *EMBO J* 25(12):2898–2910.
30. Capraro BR, et al. (2013) Kinetics of endophilin N-BAR domain dimerization and membrane interactions. *J Biol Chem* 288(18):12533–12543.
31. Simunovic M, Lee KY, Bassereau P (2015) Celebrating Soft Matter's 10th anniversary: Screening of the calcium-induced spontaneous curvature of lipid membranes. *Soft Matter* 11(25):5030–5036.
32. Prévost C, et al. (2015) IRSp53 senses negative membrane curvature and phase separates along membrane tubules. *Nat Commun* 6:8529.
33. Morlot S, et al. (2012) Membrane shape at the edge of the dynamin helix sets location and duration of the fission reaction. *Cell* 151(3):619–629.
34. Roux A, et al. (2010) Membrane curvature controls dynamin polymerization. *Proc Natl Acad Sci USA* 107(9):4141–4146.
35. Peter BJ, et al. (2004) BAR domains as sensors of membrane curvature: The amphiphysin BAR structure. *Science* 303(5657):495–499.
36. Chen H, et al. (1998) Epsin is an EH-domain-binding protein implicated in clathrin-mediated endocytosis. *Nature* 394(6695):793–797.
37. Monnier S, Rochal SB, Parmeggiani A, Lorman VL (2010) Long-range protein coupling mediated by critical low-energy modes of tubular lipid membranes. *Phys Rev Lett* 105(2):028102.
38. Golushko IY, Rochal SB, Lorman VL (2015) Complex instability of axially compressed tubular lipid membrane with controlled spontaneous curvature. *Eur Phys J E Soft Matter* 38(10):112.
39. Shlomovitz R, Gov NS, Roux A (2011) Membrane-mediated interactions and the dynamics of dynamin oligomers on membrane tubes. *New J Phys* 13:065008.
40. Simunovic M, et al. (2013) Protein-mediated transformation of lipid vesicles into tubular networks. *Biophys J* 105(3):711–719.
41. Sarić A, Cacciuto A (2012) Fluid membranes can drive linear aggregation of adsorbed spherical nanoparticles. *Phys Rev Lett* 108(11):118101.
42. Sundborger A, et al. (2011) An endophilin-dynamin complex promotes budding of clathrin-coated vesicles during synaptic vesicle recycling. *J Cell Sci* 124(Pt 1):133–143.
43. Meinecke M, et al. (2013) Cooperative recruitment of dynamin and BIN/amphiphysin/Rvs (BAR) domain-containing proteins leads to GTP-dependent membrane scission. *J Biol Chem* 288(9):6651–6661.
44. Andersson F, Löw P, Brodin L (2010) Selective perturbation of the BAR domain of endophilin impairs synaptic vesicle endocytosis. *Synapse* 64(7):556–560.
45. Ringstad N, et al. (1999) Endophilin/SH3p4 is required for the transition from early to late stages in clathrin-mediated synaptic vesicle endocytosis. *Neuron* 24(1):143–154.
46. Takei K, Slepnev VI, Haucke V, De Camilli P (1999) Functional partnership between amphiphysin and dynamin in clathrin-mediated endocytosis. *Nat Cell Biol* 1(1): 33–39.
47. Ferguson SM, et al. (2009) Coordinated actions of actin and BAR proteins upstream of dynamin at endocytic clathrin-coated pits. *Dev Cell* 17(6):811–822.
48. Daumke O, Roux A, Haucke V (2014) BAR domain scaffolds in dynamin-mediated membrane fission. *Cell* 156(5):882–892.
49. Lee E, et al. (2002) Amphiphysin 2 (Bin1) and T-tubule biogenesis in muscle. *Science* 297(5584):1193–1196.
50. Karbowski M, Jeong SY, Youle RJ (2004) Endophilin B1 is required for the maintenance of mitochondrial morphology. *J Cell Biol* 166(7):1027–1039.
51. Montes LR, Alonso A, Goñi FM, Bagatolli LA (2007) Giant unilamellar vesicles electroformed from native membranes and organic lipid mixtures under physiological conditions. *Biophys J* 93(10):3548–3554.
52. Cuvelier D, Derényi I, Bassereau P, Nassoy P (2005) Coalescence of membrane tethers: Experiments, theory, and applications. *Biophys J* 88(4):2714–2726.
53. Helfrich W (1973) Elastic properties of lipid bilayers: Theory and possible experiments. *Z Naturforsch C* 28(11):693–703.
54. Evans EA (1983) Bending elastic modulus of red blood cell membrane derived from buckling instability in micropipet aspiration tests. *Biophys J* 43(1):27–30.
55. Srivastava A, Voth GA (2013) A hybrid approach for highly coarse-grained lipid bilayer models. *J Chem Theory Comput* 9(1):750–765.
56. Plimpton S (1995) Fast parallel algorithms for short-range molecular dynamics. *J Comput Phys* 117(1):1–19.
57. Noguchi H (2014) Two- or three-step assembly of banana-shaped proteins coupled with shape transformation of lipid membranes. *Europhys Lett* 108(4).
58. Ramakrishnan N, Sunil Kumar PB, Ipsen JH (2013) Membrane-mediated aggregation of curvature-inducing nematogens and membrane tubulation. *Biophys J* 104(5): 1018–1028.